DYNAMIC SIMULATION AND EXPERIMENTAL RESEARCH OF OPEN AIR RECEIVER SYSTEM WITH CERAMIC FOAM ABSORBER

Qing Li[1], Fengwu Bai[1*], Zhifeng Wang[1], José Gonzalez Aguilar[2], Sijie Liu[3]

[1] The Key Laboratory of Solar Thermal Energy and Photovoltaic System, The Institute of Electrical Engineering Chinese Academy of Sciences, No.6 Beiertiao, Zhongguancun, Beijing100190, China,

[2] IMDEA ENERGY Institute, Avda. Ramón de la Sagra, 3 Parque Tecnológico de Móstoles E-28935 Móstoles, Madrid, Spain

[3] EDF - Asia Pacific Branch - China Division, R&D Center, Henderson Center Tower 2 Floor 12, 18 Jianguomennei Avenue, Beijing 100005, PRC

Abstract

This study investigated the heat transfer between air flow and ceramic foam absorber in open air receiver system using dynamics simulation based on Modelica language and Dymola solver. The experimental platforms of air receiver were built to validate the model, and the comparison between the experimental data and the simulation results showed this model was reliable to predict the dynamic performance of the air receiver system and to help optimize this system. The methodology of the model development and the implementation of the experiment are presented in this paper. Relied on the validated air receiver model, the sensitivity studies had been done to explore the influence of the absorber geometric parameters (thickness, mean cell size and porosity) on the volumetric ceramic foam air receiver performances. In addition, the optimization of the foam air receiver with the thermal efficiency as the objective function had been carried out based on the air receiver model and the optimization tool in Dymola.

Keywords: *Air receiver, ceramic foam, dynamic simulation, experimental validation, sensitivity studies, optimization*

1. Introduction

Due to its high concentration ratio and high efficiency, solar thermal power tower (STPT) technology has gained the worldwide attention, which is being vigorously promoted all around the world. The heat transfer fluid (HTF) used in the solar power tower system can be water, molten salt, thermal oils and air (Pavlovic et al., 2012; Romero et al., 2002). Compared with others, air as the working fluid has several advantages, such as no pollution to the environment, no phase transition, high operating temperature, no need for preheating. In the air STPT system, the air receiver plays the most significant role, which converts the concentrated solar radiation into the thermal energy of the air (Behar et al., 2013; Kribus et al., 1998). USA pioneered the first development of air receiver, which is the tube one. Since 1980s, volumetric air receivers started to be researched in Europe. The concentrated radiation flux can penetrate deeper into the volumetric air receiver due to its porosity and large extinction volume, which makes this type of air receiver more flexible than tube receiver (Avila-Marin, 2011). Refer to the material of the absorber in volumetric receiver, metal and ceramic are considered as the most appropriate materials for the high porous structure, especially silicon carbide ceramic, has large surface area, high-temperature capability, low density, and good mechanical strength, which is more suitable to be used in the high temperatures environment (Becker et al., 2006; Chavez and Chaza, 1991; Fend et al., 2004).

A lot of researches have been done numerically to study the silicon carbide ceramic foam using as the absorber in the air receiver. Some studiers focus on the macroscopic properties of the absorber based on certain simplifying assumptions. The influences brought by the air inlet velocity, the absorber porosity, the absorber thickness and mean cell size on the heat transfer performance of the receiver have been researched (Bai, 2010; Wu et al., 2011; Xu et al., 2011). Some other researchers proceed from the microscopic perspectives of the ceramic foam, and they chose to study the local heat transfer between the air flow and the solid of porous ceramic numerically (Wu et al., 2011; Wang and Pan, 2008). There are also some researchers look into the design of the ceramic foam air receiver, the optimum configuration have been found by

doi:10.18086/swc.2015.04.01 Available at http://proceedings.ises.org

comparing the thermal efficiencies and flow instabilities of volumetric absorbers with different configurations (Roldan et al., 2014).

Most researchers among them study the performances of the ceramic foam air receiver using the approaches of CFD simulation and experimental testing. Both of the two methods are time-consuming and not convenience to obtain the performance of the air receiver at all operating conditions. On the one hand, CFD simulation is commonly applied to evaluating the complex internal heat and mass transfer process, the geometry and meshing of the model should be pre-determined, which will bring the difficulty to change the parameters. On the other hand, the experimental testing is very costly to study the performance of the receiver with different designs. Therefore, dynamic modeling stands out to evaluate the sensitivity and do the optimization of the air receiver because of its convenience of changing every parameter. Up to now, some dynamic models were made to simulate the performance of the receiver in molten salt (Ferriere A, 1989) or water/steam (Xu et al., 2011; Yao et al., 2009; Yu et al., 2012) STPT. However, very few studies (Alvarez et al., 2009; Kribus et al., 2001) have focused on the dynamic simulations of the air receiver, which are indispensable for the sensitivity study and optimization on the STPT using air as HTF.

In this study, one-dimensional dynamic simulations are carried out for the ceramic foam air receiver by spatial discretization method. This modeling is based on the Modelica modeling language under Dymola software. Modelica is an object-oriented modeling language, which is freely available and has obtained high attention in recent years (Modelica Association, 2012). The ThermoSypro Library of EDF (developed by EDF and released under open source license) was used in the modeling, and the basic elements model of thermal Engineering are embodied in the ThermoSypro Library.

In order to validate the dynamic model of the air receiver, an experimental platform was set up. The receiver outlet air temperature from the experimental measurements and simulation results are compared, which shows good agreement between them.

Based on this validated air receiver model, the sensitivity studies have been done to explore the effects of the absorber geometric properties (thickness, mean cell size and porosity) on the volumetric air receiver performances. The temperature distributions for the absorber with different geometric properties are analyzed in this article. Moreover, built on the foundation of the optimization function in Dymola software, the optimal solution of geometric properties has been found with the thermal efficiency as the objective function.

2. Methodology

2.1. Physical model

Nomenclature

A	absorber surface area(m^2)	Re	Reynolds number
Cp	heat capacity (J kg^{-1} K^{-1})	T	temperatures (K)
d	mean cell diameter of the ceramic foam (m)	t	time (s)
DNI	direct normal irradiance (W m^{-2})	U	internal energy per unit volume (J m^{-3})
h	specific enthalpy(J kg^{-1})	u	superficial velocity (m s^{-1})
h_v	mean volumetric heat transfer coefficient (W m^{-3} K^{-1})	x	x-directional coordinate (m)
K_1	permeability coefficient (m^2)	y	y-directional coordinate (m)
K_2	inertial coefficient (m^{-1})	Greek symbols	
k	thermal conductivity (W m^{-1} K^{-1})	ε	porosity
L	thickness (m)	δ	Stephan Boltzmann constant (W m^{-2} K^{-4})
Nu_v	Nusselt number based on h_v	β	Rosseland mean extinction coefficient (m^{-}

			^{1})
P	pressure (Pa)	μ	dynamic viscosity (kg m^{-1} s^{-1})
q_{in}	radiation energy at inlet (W m^{-2})	ρ	density (kg m^{-3})
q_f	fluid mass flow per unit area (kg s^{-1} m^{-2})	Subscripts	
		f	fluid
q_{rad}	solid radiation force (W m^{-2})	s	solid
Q	inlet air superficial velocity (Nm^3/h)	in	inlet
$S(y)$	radiation source (W m^{-2})	out	outlet

The schematic of air receiver physical model is shown in Fig.1, where (a) is the configuration of the receiver including the insulation and ceramic foam absorber while (b) is the size and coordinate.

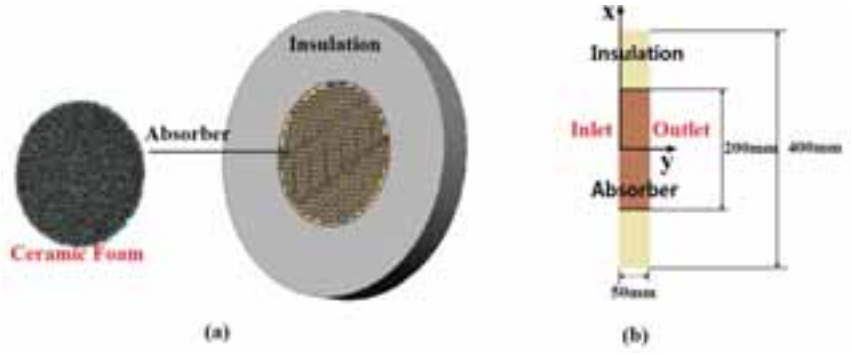

Fig. 1: Schematic of air receiver physical model: (a) configuration and (b) size and coordinates

Due to the difficulty of multidimensional simulation based on Modelica /Dymola, one dimension model was established by spatial discretization along the air flow direction (y-axis direction). The insulation was ignored in this model.

Air properties were defined as temperature dependent in this model, including the heat capacity, the density, the viscosity and the thermal conductivity because of the high working temperature of the receiver.

2.2. Numerical model

The following assumptions are made in order to simplify the problem. (1) The ceramic foam absorber is isotropic. (2) The air mass flow and the solar incident radiation flux are uniform on the surface of the absorber. (3) The heat insulation of the receiver is very well and the heat loss from the cylindrical out surface is ignored.

For spatial discretization, a number of sections are divided along the fluid flow direction. The energy conservation of section i is represented in Fig.2, including the conductive heat transfer inside air, the radiative and conductive heat transfer of the internal solid, the convective heat transfer between air and solid, and the penetrating solar energy source. Moreover, the convective and radiative heat losses at the air entrance surface are also embodied in the first section.

The energy conservation equations of solid and fluid are presented in eq. 1 and eq. 2, respectively.

For solid:

$$\frac{\partial\left[(1-\varepsilon)\cdot k_s\cdot\frac{\partial T_S}{\partial y}\right]}{\partial y}-\frac{\partial q_{rad}}{\partial y}-h_v\cdot(T_s-T_f)+\frac{\partial S(y)}{\partial y}=\rho_s\cdot(1-\varepsilon)\cdot Cp_s\cdot\frac{\partial T_S}{\partial t} \qquad \text{(eq. 1)}$$

For fluid:

$$\frac{\partial\left(\varepsilon\cdot k_f\cdot\frac{\partial T_f}{\partial y}\right)}{\partial y}+h_v\cdot(T_s-T_f)-\frac{\partial(q_f\cdot h_f)}{\partial y}=\frac{\partial U_f}{\partial t}\cdot\varepsilon \qquad \text{(eq. 2)}$$

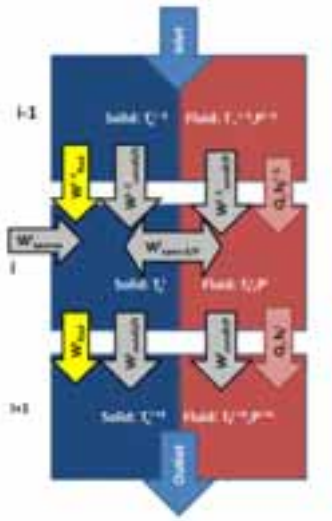

Fig. 2: Energy balance in absorber

In the equations, *S(y)* stands for the distribution of concentrated radiation flux inside the ceramic foam absorber as an exponential decay displayed in eq. 3 (Coquard et al., 2009). U_f represents the air internal energy expressed by eq. 4. q_{rad} means the radiation heat transfer in solid which plays a significant role as the absorber working at high temperature. According to the Rosseland radiation model, q_{rad} is determined using Eq. (5) (Cherif and Sifaoui, 2005; Zhao et al., 2004). β is the extinction coefficient of the ceramic foam, which can obtained by eq. 6 (Petrasch et al., 2007).

$$S(y) = q_{in} \cdot e^{-(\beta \cdot y)} \quad \text{(eq. 3)}$$

$$\frac{\partial U_f}{\partial t} = \left(\rho_f + h_f \cdot \frac{\partial \rho_f}{\partial h_f}\Big|_p\right) \cdot \frac{\partial h_f}{\partial t} + \left(h_f \cdot \frac{\partial \rho_f}{\partial P}\Big|_{h_f} - 1\right) \cdot \frac{\partial P}{\partial t} \quad \text{(eq. 4)}$$

$$q_{rad} = -\frac{16\delta \cdot T_s^3}{3\beta} \cdot \frac{\partial T_s}{\partial y} \quad \text{(eq. 5)}$$

$$\beta = \frac{0.56}{d} \quad \text{(eq. 6)}$$

The volumetric convective heat transfer coefficient between the air and the solid (h_v) is defined as a variation with the Nusselt number as eq. 7， which can be derived from eq. 8 and eq. 9 (Fu et al., 1998).

$$h_v = Nu_v \cdot \frac{k_f}{d^2} \quad \text{(eq. 7)}$$

$$Nu_v = \left(0.0426 + 1.236\frac{d}{L}\right) \cdot Re \quad \text{(eq. 8)}$$

($2 < Re < 836$)

$$Re = \frac{d \cdot u_f \cdot \rho_f}{\mu_f} \quad \text{(eq. 9)}$$

The expression of the pressure loss in the absorber is shown in eq. 10 – eq. 12 according to the classic Darcye-Forchheimer law (Moreira et al., 2004).

$$-\frac{\Delta P}{y} = \frac{\mu_f}{K_1} \cdot u_1 + 0.5K_2 \cdot \rho_f \cdot u_f^2 \quad \text{(eq. 10)}$$

$$K_1 = \frac{d^2}{150} \cdot \frac{\varepsilon^3}{(1-\varepsilon)^2} \quad \text{(eq. 11)}$$

$$K_2 = \frac{3.5}{d} \cdot \frac{1-\varepsilon}{\varepsilon^3} \quad \text{(eq. 12)}$$

Besides, the functions in ThermoSypro Library are used to obtain the variations of air's physical parameters, such as the heat capacity, the density, the viscosity and the thermal conductivity with corresponding air

temperatures and pressures.

3. Experimental validation

The experimental platform was set up in Badaling solar thermal power experimental base of China for validating the receiver model. The schematic diagram and one photograph of the experimental system are depicted in Fig. 3, and the system is compose of the solar furnace, air receiver, cooling device, draught fan and measuring devices. Air receiver of 200mm length is the key component of the system, which consists of the 50mm absorber, the 150mm cavity for air flow mixing, the insulation layer and the supporting component. The cooling device was used to cool the hot air to protect the draught fan and other devices, which was made up of a tank of honeycomb ceramic bulks.

Two thermocouples were installed on the central axis of the receiver 160 mm and 180 mm behind the front surface of the absorber to measure the receiver outlet air temperature. Since the input solar flux was not uniform, the air temperature distribution inside the absorber was not uniform in the radial direction. However, the air leaving the absorber was assumed to be thoroughly mixed 150 mm behind the front surface of the absorber which can be proved by that the temperatures of the two thermocouples differed by less than 5 K. Thus, the average temperature of these two thermocouples was used as the experimental receiver outlet air temperature.

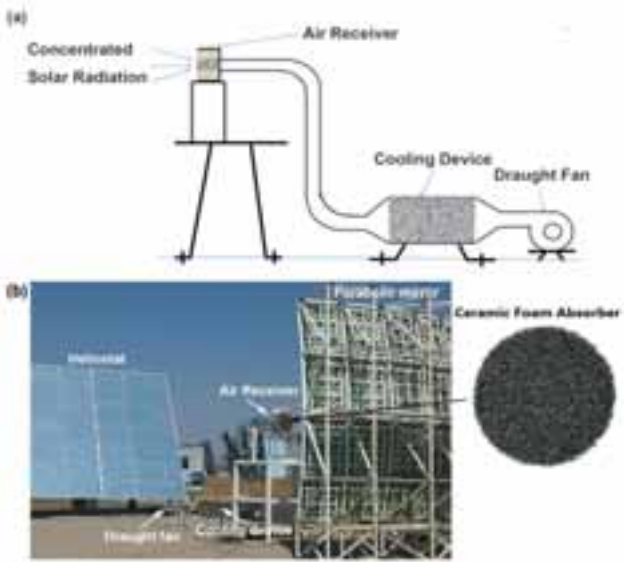

Fig. 3: Experiment system of air receiver: (a) schematic diagram and (b) system photograph

The solar radiation flux at the air receiver inlet surface is determined by the data tested through the "charge coupled device (CCD) camera + moving bar" indirect measurement, which is used as the inlet boundary condition in the dynamic simulation. The porosity, mean cell size, and thickness of the ceramic foam absorber are 0.65, 2.5 mm and 50mm, respectively. The air mass flow during the experiment was adjusted at 60Nm^3/h (the inlet air superficial velocity is 0.53m/s). The parameters of the absorber and the inlet air superficial velocity used in the dynamic simulation were set identical to the values in the experiment. The comparison between experimental measurements and simulation results of the air temperature at receiver outlet is shown in Fig. 4. The upper curve presents the DNI (direct normal irradiance) during the experiment time. DNI, solar radiation flux and air mass flow are the three inputs of the simulation model, which are achieved from the experiments. The receiver outlet air temperatures over time, obtained from experiment and simulation result, are depicted in the below diagram. We can see that the simulated outlet air temperature is in appreciable agreement with the experimental data, both of which show gentler variations than DNI. It can be concluded that the error between the two curves is less than 10%, mainly due to the limitations of the 1-D approach for the 3-D process, the discretization and round-off errors in the calculations, the uncertainties in the heat transfer coefficient model and radiation transfer functions and the measurement errors in the vortex

flow meter and the thermocouples. The vortex flow meter, model LUGBZ-40, had an accuracy of ±1.5% FS according to the manufacturer and the K type thermocouples used in the experiment had accuracies of ±2.5 K within the measurement range of 300-1000 K. Compared to experiments, using dynamic modeling approach can be more applicable for the investigation and optimization of the air receiver since it is more convenient to change the date of the receiver parameters such as the thickness, the mean cell size and the porosity.

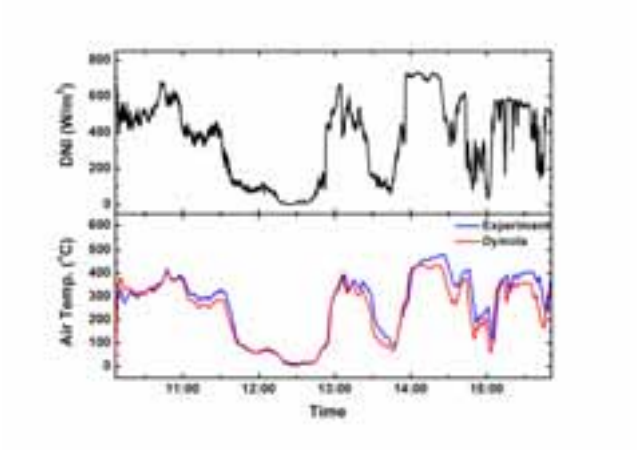

Fig. 4: Comparison between experimental measurements and simulation results of the outlet air temperature in air receiver system

4. Sensitivity studies

In order to research the influence of the structure of the absorber, we conducted a series of sensitivity study of the thickness, the mean cell size and the porosity of the ceramic foam absorber. The validated air receiver model described in this paper is the fundamental of these sensitivity studies. The inlet air superficial velocity is set as a constant value of 0.53m/s, and the inlet air temperature is 20°C. Also, we fix the concentrated solar radiation flux as 500 kW/m^2 in all the cases of this section. Under the same inlet air superficial velocity, inlet air temperature and incident energy flux, the thermal efficiencies for different cases can be reflected by the corresponding outlet air temperatures.

4.1. Effects of thickness

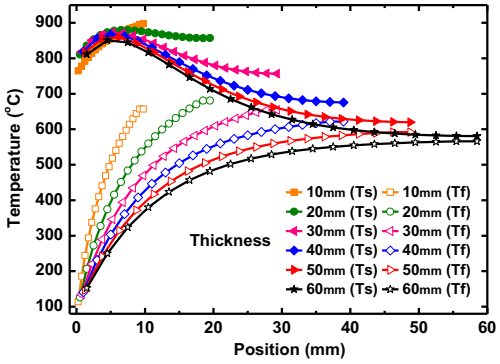

Fig. 5: The temperature distributions for different thicknesses

Fig. 5 shows the steady-state temperature distributions of the solid and fluid phase with different thickness but same porosity and mean cell size of the absorber (d = 3mm, ε = 0.5). As described in this figure, when the thickness is greater than 20mm, the fluid temperature decreases with the increasing of the thickness. Since the input power is fixed, the increase of the thickness will bring the decrease of the average volumetric heat power, which will reduce the fluid temperature. Another reason is that the volumetric convective heat transfer coefficient between the air and the solid will decrease with the increasing of the thickness, due to eq.

8, and it will decrease the heat exchange ability between air and solid. From the figure, we also can see the solid temperature at the outlet decreases with the increasing of the thickness. The reason is that the solid thermal resistance increases with the increasing of the thickness, which causes the large temperature drop of the solid. In addition, the temperature difference between the solid and air at the outlet decreases with the increasing of the thickness, that because the thicker the absorber is , the longer the heat exchange time and distance between fluid and solid are.

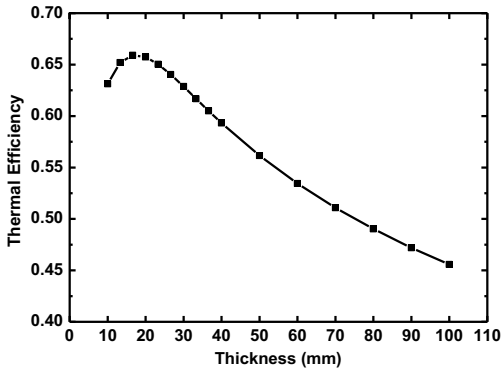

Fig. 6: The thermal efficiencies for different thicknesses on steady state

Fig. 6 is the thermal efficiencies at steady state with different absorber thicknesses but same porosity and mean cell size of the absorber (d = 3mm, ε= 0.5). It is can be seen in this figure, the thermal efficiency increases firstly and then decreases with the increasing of thickness, which comes highest when the thickness is 18mm. As mentioned before, the thermal efficiencies can be reflected by the outlet air temperatures under the same inlet air superficial velocity, inlet air temperature and incident energy flux, as eq.13. When the absorber thickness is rather small, the time of the air flow through the absorber will be very short, which caused the insufficiency of the heating and the reduction of the air outlet temperature. And also if the thickness is small enough, the solar radiation energy will penetrate out of the absorber, which will bring more heat loss. When the thickness is greater than 18mm, the fluid temperature will decrease with the increasing of the thickness. One reason is that the increasing of the thickness brings the reduction of the volumetric convective heat transfer coefficient between the air and the solid, as eq. 8, and the heat exchange ability between air and solid will drop. Another reason is that the solid temperature at the outlet decreases with the increasing of the thickness.

$$\eta = \frac{Q\cdot\left[\left(h_{f\,out}-\frac{P_{out}}{\rho_{f\,out}}\right)-\left(h_{f\,in}-\frac{P_{in}}{\rho_{f\,in}}\right)\right]}{q_{in}\cdot A} \qquad \text{(eq. 13)}$$

4.2. Effects of mean cell size

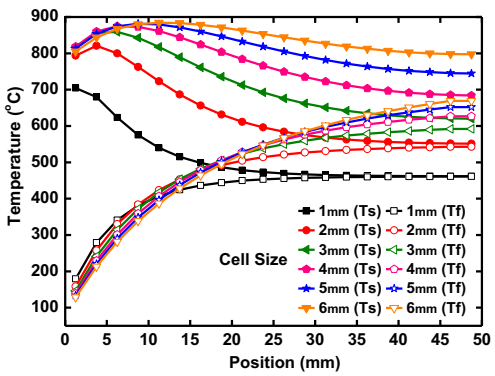

Fig. 7: The temperature distributions for different mean cell sizes

Fig. 7 shows the temperature distributions of the solid and fluid phase with same thickness and porosity of the absorber (L = 50mm, ε = 0.5) but different thickness at steady state. It can be seen in this figure that both the solid and fluid temperatures increase with the increasing of the mean cell size. According to eq. 6, the extinction coefficient of the absorber is inversely proportional to the mean cell size, means the bigger the mean cell size is, the small the extinction coefficient is, the more solar energy will penetrate into the absorber, which makes the increasing of the solid and fluid temperatures. From Fig. 7, we also can see the temperature difference between the solid and air at the outlet increases with the increasing of the mean cell size. The reason is that the volumetric convective heat transfer coefficient between the air and the solid decreases with the increasing of the mean cell size, as eq. 7.

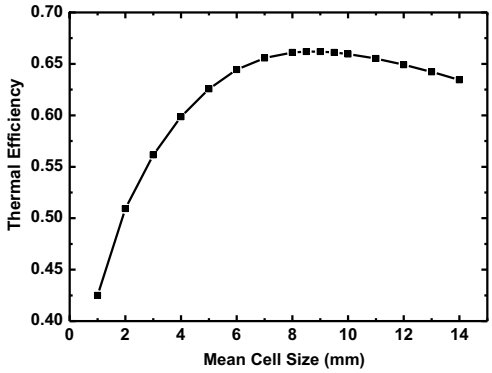

Fig. 8: The thermal efficiencies for different mean cell sizes on steady state

Fig. 8 is the thermal efficiencies at steady state with different mean cell sizes but same thickness and porosity of the absorber (L = 50mm, ε = 0.5). It is can be seen in this figure, the thermal efficiency increases first and then decreases with the increasing of mean cell size, which comes highest when the mean cell size is 8mm with the fixed inlet air superficial velocity, inlet air temperature, incident energy flux, absorber porosity, and absorber thickness. The reason is that when the mean cell size of the absorber is too big, the volumetric convective heat transfer coefficient between the air and the solid will be very small, and the heat exchanging capacity between air and solid will become weak, which will cause the decreasing of the air outlet temperature.

4.3. Effects of porosity

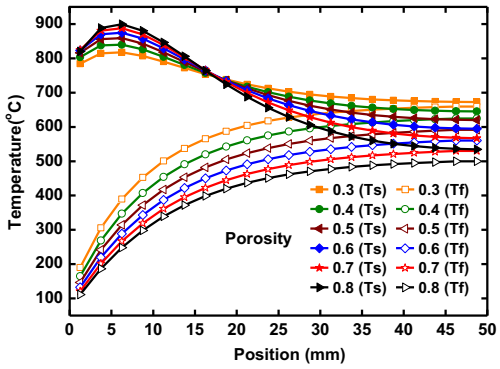

Fig. 9: The temperature distributions for different porosities

Fig. 9 shows the steady-state temperature distributions of the solid and fluid phase with different porosities but same thickness and mean cell size of the absorber (L = 50mm, d= 3mm). As we can see, the front solid temperatures of the absorbers with large porosities are higher than the temperatures of the absorbers with small porosities while the rear solid temperatures of the absorbers with large porosities are lower at the same position. The reason is that the solid of the absorber with large porosity is lighter, thus, the temperature of the

front solid is higher for absorbing the same incident energy. On the other side, the higher front temperature brings more heat loss on the surface of the receiver. It results in the reduction of the total energy penetrate into the receiver system, which makes the temperatures of the rear solid and the fluid relatively lower. The figure also shows that the solid temperature gradient of the absorber with large porosity is greater, which is owing to the larger solid thermal resistance. The larger the porosity is, the smaller the solid cross-sectional area is, and the larger the solid thermal resistance is. Furthermore, what we also can obtain from Fig. 9 is that the temperature difference between the solid and air at the outlet increases with the increasing of the porosity. The reason is that the lower air temperature makes the Reynolds number and the thermal conductivity decrease. According to eq. 7-eq. 9, the volumetric convective heat transfer coefficient between the air and the solid decreases with the lower air temperature, this makes the temperature difference between the solid and air at the outlet increases with the increase.

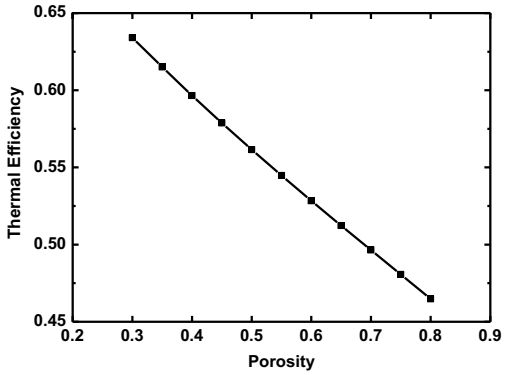

Fig. 10: The thermal efficiencies for different porosities on steady state

Fig. 10 is the thermal efficiencies at steady state with different porosities but same thickness and mean mean cell size of the absorber (L= 50mm, d= 3mm). It is can be seen in this figure, the thermal efficiency decreases with the increasing of the porosity. As explained before, larger porosity brings smaller solid cross-sectional area and larger thermal resistance in solid. And the larger thermal resistance causes greater temperature gradient in the solid, which results in the lower outlet solid and air temperatures. According to eq.13, the thermal efficiency also decreases with the increasing of the porosity as the outlet air temperature under the same inlet air superficial velocity, inlet air temperature and incident energy flux. Despite the smaller porosity can bring the greater the thermal efficiency, but considering the pressure drop and manufacture feasibility issues, the porosity should be kept in an appropriate range.

For the purpose of studying the influential factors of the heat transfer in the ceramic foam, the return air system is not considered in the model, which plays an important role in integrity and performance of open volumetric air receiver. Thus, the above-mentioned observations will be extended into the open volumetric air receiver integrated with the air return loop, based on the updated model in the future.

5. Optimization

The outlet air temperature and thermal efficiency at steady state are the most important indicators of air receiver performance, both of which are decided by the following five parameters: the solar radiation flux, the inlet air superficial velocity, the absorber thickness, the absorber mean cell size and the absorber porosity. In this section, we conduct the optimization of the air receiver system (without air return system) based on the air receiver model established in this article, and with the help of the optimization tool in Dymola software. Limited by the function of the Dymola software, we can only do the optimization on three parameters at most. Therefore, firstly we choose several different cases depend on the different solar radiation fluxes and inlet air superficial velocities. For each case, the optimal absorber geometric parameters (thickness, mean cell size and porosity) to achieve the maximum thermal efficiency are found, respectively. Table 1 shows the setting of the optimized parameters. Taking into account the feasibility of the manufacture, we define the ranges of these three parameters.

Tab. 1: Parameter setting of the optimization

Parameter	Minimum	Maximum	Unit
Thickness	10	100	mm
Mean cell size	1	6	mm
Porosity	0.3	0.8	1

Table 2 shows the optimization results under the same inlet air superficial velocity, as 0.53m/s, but with different solar radiation fluxes. As we can see, for various solar radiation fluxes, the optimized values of the absorber geometric parameters are the same. The highest outlet air temperature of the receiver increases with the increasing of the solar radiation flux, while the maximum thermal efficiency decreases with the increasing of the solar radiation flux.

Tab. 2: Optimization result with different solar radiation fluxes and fixed inlet air superficial velocity

Inlet air superficial velocity: 0.53m/s					
Solar radiation flux (kW/m^2)	400	450	500	550	600
Thickness (mm)	24.86	24.86	24.86	24.86	24.86
Mean cell size (mm)	4.09	4.09	4.09	4.09	4.09
Porosity	0.3	0.3	0.3	0.3	0.3
Pressure drop (Pa)	3753.70	3995.29	4222.97	4437.31	4639.05
Highest outlet air temperature (^{o}C)	618	674	727	775	821
Maximum thermal efficiency	0.737	0.722	0.707	0.692	0.677

Table 3 shows the optimization results under different inlet air superficial velocities, but with same solar radiation flux (500 kW/m^2). It can be seen from the table, for various inlet air superficial velocities, the optimized values of the absorber geometric parameters are almost the same. The highest outlet air temperature of the receiver decreases with the increasing of the inlet air superficial velocity, while the maximum thermal efficiency decreases with the increasing of the inlet air superficial velocity.

Tab. 3: Optimization result with different inlet air superficial velocities and fixed solar radiation flux

Solar radiation flux: 500 kW/m^2					
Inlet air superficial velocity (m/s)	0.35	0.44	0.53	0.62	0.71
Thickness (mm)	26.04	24.49	24.86	24.49	25.45
Mean cell size (mm)	4.06	4.11	4.09	4.11	4.07
Porosity	0.3	0.3	0.3	0.3	0.3
Pressure drop (Pa)	2514.22	3188.98	4222.97	5133.03	6558.83
Highest outlet air temperature (^{o}C)	870	772	727	628	564
Maximum thermal efficiency	0.608	0.681	0.707	0.751	0.771

Since the optimal geometric parameters for various solar radiation fluxes and inlet air superficial velocities are almost the same, we fixed the thickness, the mean cell size and porosity of the ceramic foam absorber as 25mm, 4.09 mm and 0.3, respectively; and we do the optimization of the solar radiation flux and inlet air superficial velocity to find the optimum condition to obtain the maximum thermal efficiency on the premise of the outlet air temperature is 800 ^{o}C. In consideration of the concentration ratio and the pressure loss, the ranges of the solar radiation flux and inlet air superficial velocity are limited as 0-2 m/s and 0-2000 kW/m^2. The result in Table 4 represents that when the solar radiation flux is 1825 kW/m^2 the inlet air superficial velocity is 1.75m/s, the maximum thermal efficiency of 0.769 can be achieved.

Tab. 4: Optimization result with fixed absorber geometric parameters and outlet air temperature

Thickness: 25mm, mean cell size:4.09mm, porosity:0.3, outlet air temperature: 800 ^{o}C			
Solar radiation flux (0-2000 kW/m2)	Inlet air superficial velocity (0-2 m/s)	Maximum thermal efficiency	Pressure drop (Pa)
1825 kW/m^2	1.75m/s	0.769	67885

The corresponding pressure drops are also depicted in the optimization result tables, which agree with the results in (Bai, 2010). The pressure drop in the ceramic foam is not the research emphasis of this paper.

6. Conclusions

In this article, the dynamic simulation model of ceramic foam open-loop air receiver, which is the most principal components in STPT using air as the HTF, was established using the object-oriented language Modelica based on Dymola simulation environment. The experiments of the air receiver had been carried out for the model validation, and the simulation results agree well with the experiment data. The sensitivity studies show that the absorber geometric properties (thickness, mean cell size and porosity) have distinct influences on the solid and fluid temperature distributions and the thermal efficiencies of the ceramic foam air receiver. The combination values of the absorber mean cell size, porosity, thickness, solar radiation flux and inlet air superficial velocity in certain ranges to achieve the highest thermal efficiency on the premise of the outlet air temperature is 800 ^{o}C were found by the optimization method using the receiver model.

In conclusion, this experiment validated model is reliable to predict the dynamic performance of the ceramic foam air receiver and can be used for receiver optimization in different STPT systems using this type of air receiver.

7. Acknowledgements

The present work was supported by National Natural Scientific Foundation of China (Grant No. 51376176).The research leading to these results has also received funding from the European Union Seventh Framework Program FP7/2007-2013 under grant agreement No.609837.

8. References

Alvarez, J.D., Guzman, J.L., Yebra, L.J., Berenguel, M., 2009. Hybrid modeling of central receiver solar power plants. Simul. Model Pract. Th. 17 (4), 664-679.

Avila-Marin, A.L., 2011. Volumetric receivers in Solar Thermal Power Plants with Central Receiver System technology: A review. Sol. Energy 85 (5), 891-910.

Bai, F.W., 2010. One dimensional thermal analysis of silicon carbide ceramic foam used for solar air receiver. Int. J. Therm. Sci. 49 (12), 2400-2404.

Becker, M., Fend, T., Hoffschmidt, B., Pitz-Paal, R., Reutter, O., Stamatov, V., Steven, M., Trimis, D., 2006. Theoretical and numerical investigation of flow stability in porous materials applied as volumetric solar receivers. Sol. Energy 80 (10), 1241-1248.

Behar, O., Khellaf, A., Mohammedi, K., 2013. A review of studies on central receiver solar thermal power plants. Renew. Sust. Energ. Rev. 23 12-39.

Chavez, J.M., Chaza, C., 1991. Testing of a Porous Ceramic Absorber for a Volumetric Air Receiver. Sol. Energ. Mater. 24 (1-4), 172-181.

Cherif, B., Sifaoui, M.S., 2005. Numerical study of heat transfer in an optically thich semi-transparent spherical porous medium. J Quant Spectrosc Ra 91(3), 363-372.

Coquard, R., Rochais, D., Baillis, D., 2009. Experimental investigations of the coupled conductive and radiative heat transfer in metallic/ceramic foams. Int. J. Heat Mass Tran. 52 (21-22), 4907-4918.

Fend, T., Hoffschmidt, B., Pitz-Paal, R., Reutter, O., Rietbrock, P., 2004. Porous materials as open volumetric solar receivers: Experimental determination of thermophysical and heat transfer properties. Energy 29 (5-6), 823-833.

Ferriere A, B.B., 1989. Development of an optical control strategy for the Themis solar plant: Part I - Themis transient model. Journal of Solar Energy Engineering 111 298 -303.

Fu, X., Viskanta, R., Gore, J.P., 1998. Measurement and correlation of volumetric heat transfer coefficients of cellular ceramics. Exp. Therm. Fluid Sci. 17 (4), 285-293.

Kribus, A., Doron, P., Rubin, R., Reuven, R., Taragan, E., Duchan, S., Karni, J., 2001. Performance of the directly-irradiated annular pressurized receiver (DIAPR) operating at 20 bar and 1,200 degrees C. J. Sol.

Energ-T. Asme. 123 (1), 10-17.

Kribus, A., Zaibel, R., Carey, D., Segal, A., Karni, J., 1998. A solar-driven combined cycle power plant. Sol. Energy 62 (2), 121-129.

Modelica Association, 2012. Modelica. a unified object-oriented language for physical systems modeling.

Moreira, E.A., Innocentini, M.D.M., Coury, J.R., 2004. Permeability of ceramic foams to compressible and incompressible flow. J. Eur. Ceram. Soc. 24 (10-11), 3209-3218.

Pavlovic, T.M., Radonjic, I.S., Milosavljevic, D.D., Pantic, L.S., 2012. A review of concentrating solar power plants in the world and their potential use in Serbia. Renew. Sust. Energ. Rev. 16 (6), 3891-3902.

Petrasch, J., Wyss, P., Steinfeld, A., 2007. Tomography-based Monte Carlo determination of radiative properties of reticulate porous ceramics. J. Quant. Spectrosc Ra. 105 (2), 180-197.

Roldan, M.I., Smirnova, O., Fend, T., Casas, J.L., Zarza, E., 2014. Thermal analysis and design of a volumetric solar absorber depending on the porosity. Renew. Energ. 62 116-128.

Romero, M., Buck, R., Pacheco, J.E., 2002. An update on solar central receiver systems, projects, and technologies. J. Sol. Energ-T. Asme. 124 (2), 98-108.

Wang, M., Pan, N., 2008. Modeling and prediction of the effective thermal conductivity of random open-cell porous foams. Int. J. Heat Mass Tran. 51 (5-6), 1325-1331.

Wu, Z.Y., Caliot, C., Flamant, G., Wang, Z.F., 2011. Coupled radiation and flow modeling in ceramic foam volumetric solar air receivers. Sol. Energy 85 (9), 2374-2385.

Wu, Z.Y., Caliot, C., Flamant, G., Wang, Z.F., 2011. Numerical simulation of convective heat transfer between air flow and ceramic foams to optimise volumetric solar air receiver performances. Int. J. Heat Mass Tran. 54 (7-8), 1527-1537.

Xu, C., Song, Z., Chen, L.D., Zhen, Y.A., 2011. Numerical investigation on porous media heat transfer in a solar tower receiver. Renew. Energ. 36 (3), 1138-1144.

Xu, E.S., Yu, Q.A., Wang, Z.F., Yang, C.Y., 2011. Modeling and simulation of 1 MW DAHAN solar thermal power tower plant. Renew. Energ. 36 (2), 848-857.

Yao, Z.H., Wang, Z.F., Lu, Z.W., Wei, X.D., 2009. Modeling and simulation of the pioneer 1 MW solar thermal central receiver system in China. Renew. Energ. 34 (11), 2437-2446.

Yu, Q., Wang, Z.F., Xu, E., 2012. Simulation and analysis of the central cavity receiver's performance of solar thermal power tower plant. Sol. Energy 86 (1), 164-174.

Zhao, C.Y., Lu, Y.J., Hodon, H.P., 2004. Thermal radiation in untralight metal foams with open cells. Int J Heat Mass Tran 47(14-16), 2927-2939.